Sensitive dependence of the motion of a legged robot on granular media

Chen Li[a], Paul B. Umbanhowar[b], Haldun Komsuoglu[c], Daniel E. Koditschek[c], and Daniel I. Goldman[a,1]

[a]School of Physics, Georgia Institute of Technology, Atlanta, GA 30332; [b]Department of Mechanical Engineering, Northwestern University, Evanston, IL 60208; and [c]Department of Electrical and Systems Engineering, University of Pennsylvania, Philadelphia, PA 19104

Legged locomotion on flowing ground (e.g., granular media) is unlike locomotion on hard ground because feet experience both solid- and fluid-like forces during surface penetration. Recent bioinspired legged robots display speed relative to body size on hard ground comparable with high-performing organisms like cockroaches but suffer significant performance loss on flowing materials like sand. In laboratory experiments, we study the performance (speed) of a small (2.3 kg) 6-legged robot, SandBot, as it runs on a bed of granular media (1-mm poppy seeds). For an alternating tripod gait on the granular bed, standard gait control parameters achieve speeds at best 2 orders of magnitude smaller than the 2 body lengths/s ($\approx$60 cm/s) for motion on hard ground. However, empirical adjustment of these control parameters away from the hard ground settings restores good performance, yielding top speeds of 30 cm/s. Robot speed depends sensitively on the packing fraction ϕ and the limb frequency ω, and a dramatic transition from rotary walking to slow swimming occurs when ϕ becomes small enough and/or ω large enough. We propose a kinematic model of the rotary walking mode based on generic features of penetration and slip of a curved limb in granular media. The model captures the dependence of robot speed on limb frequency and the transition between walking and swimming modes but highlights the need for a deeper understanding of the physics of granular media.

bioinspired robotics | robotic gait | locomotion on complex terrain | volume fraction | sand

Compared with agile terrestrial organisms, most man-made vehicles possess limited mobility on complex terrain (1) and are easily thwarted by materials like rubble and sand. Increased locomotive performance of engineered platforms demands better understanding of interaction with complex environments. At the same time, there is increasing evidence that small legged machines can have greater maneuverability than large wheeled vehicles in many natural environments (2). However, although wheeled and treaded locomotion on sand has been well studied by pioneers like Bekker (3), study of the interaction of animals or legged devices with complex media like sand is in its infancy (4), in part because the physics of penetration and drag in granular media is largely unexplored for realistic conditions. Nearly all previous experiments and models of terrestrial locomotion were developed for running and walking on rigid, flat, nonslip substrates in which the possibility of substrate flow was ignored (5–9).

Rainforest, grassland, polar tundra, mountains, and desert are examples of complex Earth terrains with flowing substrates that challenge locomotors; the limited experience of the Mars Rovers supports the presumption that extraterrestrial landscapes will be even more daunting. Deserts, common in nature and occupying $\approx$10% of land surface on Earth (10), consist largely of granular media, a representative complex substrate. Granular materials, defined as collections of discrete particles, can exhibit solid-like behavior below a critical yield stress (11, 12), whereas fluid-like (13), gas-like (14), and even glass-like (15) behaviors are possible during flow. Yet, compared with other complex materials like

debris, mud, or snow, granular materials are simple enough that fundamental understanding of the collective physics can be achieved through interplay of experiment and theory. Unlike more heterogeneous real-world environments, granular media can be precisely controlled using laboratory scale devices (15, 16) to create states of varying material strength that mimic different deformable flowing materials produced during locomotion on complex terrains. Here, we systematically explore the performance of a small legged device, SandBot, on granular media prepared in different packing states with volume fraction ranges typical of desert sand (40). Despite SandBot's [and its predecessor RHex's (17)] ability to move nimbly and rapidly over a wide range of natural terrain, we find that on granular media, the locomotion is remarkably sensitive to substrate preparation and gait characteristics, which points to both the need for a more sophisticated understanding of the physics of motion within granular media and the possibility of better robotic design and control paradigms for locomotion on complex terrains.

Results and Discussion

The robot we study, SandBot (Fig. 1A), is the smallest (mass 2.3 kg) in a successful series of biologically inspired (18) hexapedal robots, the RHex class (17). RHex incorporates the pogo stick-like dynamics observed in a diversity of biological organisms running on hard ground (19). This dynamics, called the spring-loaded inverted pendulum (SLIP) template (41), is hypothesized to confer passive self-stabilization properties to both biological and robotic locomotors (20). RHex was the first legged machine to achieve autonomous locomotion at speeds >1 body length/s (17), and it and its "descendants" such as EduBot/SandBot, Whegs (21), and iSprawl (22) are still the leaders in legged mobility (roughly, speed and efficacy) on general terrain. In fact, before the recent development of the much larger BigDog (23) platform (1 m long, 75 kg), RHex remained the only class of legged machine with documented ability to navigate on complex, natural, outdoor terrain of any kind and has been used as the standard legged platform in comparisons with commercial wheeled and tracked vehicles like Packbot (24).

SandBot moves using an alternating tripod gait in which 2 sets of 3 approximately c-shaped legs rotate synchronously and π out of phase. A clock signal (Fig. 1C), defined by 3 gait parameters (see *Materials and Methods*), prescribes the angular trajectory of each tripod. The c-legs distribute contact (25) over their surfaces and allow the robot to move effectively on a variety of terrain.
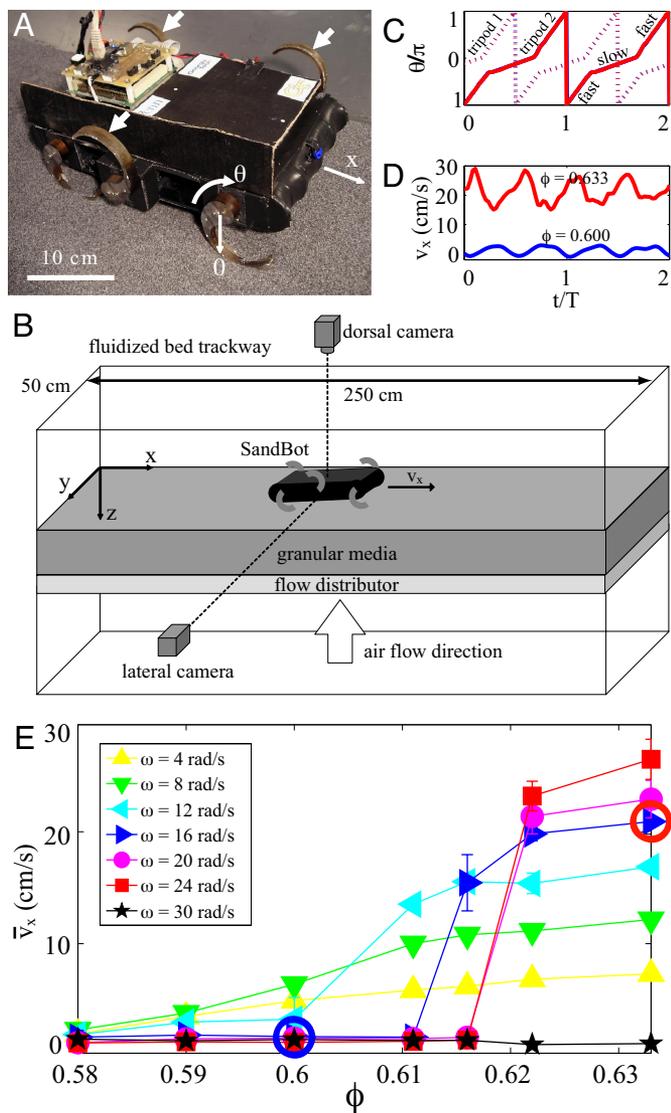
PHYSICS

Fig. 1. Locomotion of a legged robot on granular media is sensitive to substrate packing and limb frequency. (*A*) The 6-legged robot, SandBot, moves with an alternating tripod gait (alternate triplets of limbs rotate π out of phase); arrows indicate members of 1 tripod. (*B*) Pulses of air through the bottom of the fluidized bed trackway control the initial volume fraction ϕ of the granular substrate; air is turned off before the robot begins to move. (*C*) Tripod leg-shaft angle θ vs. time is controlled to follow a prescribed trajectory with 2 phases: a slow stance phase and a fast swing phase. Overlapping trajectories from trials with $\phi = 0.633$ (red) and $\phi = 0.600$ (blue) at limb frequency $\omega = 16$ rad/s demonstrate that the controller maintains the desired kinematics independent of material state. (*D*) Identical tripod trajectories produce different motion for $\phi = 0.633$ (red) and $\phi = 0.600$ (blue). (*E*) For fixed limb frequency ($\omega = 4, 8, 12, 16, 20, 24,$ and 30 rad/s) the robot speed is remarkably sensitive to ϕ. Red and blue circles show the corresponding states in *C* and *D*.

On rigid, no-slip ground, SandBot's limb trajectories are tuned to create a bouncing locomotion (17) that generates speeds up to 2 body lengths/s (≈ 60 cm/s). We tested this clock signal on granular media but found that the robot, instead of bouncing, adopts a swimming gait in which the legs always slip backward relative to the stationary grain bed and for which performance is reduced by a factor of 30 to ≈ 2 cm/s [see supporting information (SI) Movie S1]. We surmised that this was due to an interval of double stance (both tripods in simultaneous contact with the ground), which is useful on hard ground during bounc-

ing gaits but apparently causes tripod interference on granular media. Changing the clock signal to remove the double stance allowed SandBot to move (see Movie S2) in the granular media at speeds up to 1 body length/s (≈ 30 cm/s) in a rotary walking gait that resembles the pendular gait of the robot on hard ground (26) but with important kinematic differences (discussed below). No amount of clock signal adjustment produced rapid bouncing locomotion on granular media. We hypothesize that the $\approx 50\%$ decrease in top speed relative to hard ground is associated with the inability of the robot to undergo the aerial phases associated with the bouncing gait. Study of biological locomotion has revealed a similar loss of performance and has shown that speeds of desert-adapted lizards like *Callisaurus draconoides* on granular media are typically 75% of top speeds on hard ground.

In the desert, animals and man-made devices can encounter granular media which exist in a wide range of volume fractions (40), and some desert adapted animals (like lizards) can traverse a range of granular media with little loss in performance (16). To test the robot performance on controlled volume fraction granular media, we employ a 2.5-m-long fluidized bed trackway (Fig. 1*B*) (27), which allows the flow of air through a bed of granular media, in this case ≈ 1-mm poppy seeds. With initial fluidization followed by repeated pulses of air (28), we prepare controlled volume fraction states with different penetration properties (29). In this study, we test the performance (forward speed v_x) of SandBot with varied limb angular frequency (ω) for volume fraction (ϕ) states ranging from loosely to closely packed ($\phi = 0.580$ to $\phi = 0.633$) which fall in the range of ϕ observed in desert dunes (40). We chose forward speed as a metric of performance because it could be readily measured by video imaging. We hypothesized that limb frequency would be important to robot locomotion because the substrate yield strength increases with volume fraction and the yield stress × robot limb area divided by the robot mass × velocity is proportional to the maximum limb frequency for efficient locomotion.

We find that robot speed is remarkably sensitive to ϕ (see Movie S3). For example, at $\omega = 16$ rad/s, $v_x(t)$ shows a change in average speed $\bar{v}_x$ of nearly a factor of 5 as ϕ changes by just 5% (Fig. 1 *D* and *E*). For a closely packed state ($\phi = 0.633$), $\bar{v}_x \approx 20$ cm/s with 5-cm/s oscillations during each tripod rotation, whereas for a more loosely packed state ($\phi = 0.600$), $\bar{v}_x \approx 2$ cm/s with 1-cm/s oscillations.

This sensitivity to volume fraction is shown in the average robot speed vs. volume fraction (Fig. 1*E*). For fixed ω, $\bar{v}_x$ is effectively constant for ϕ above a critical volume fraction $\phi_c(\omega)$, but is close to zero for $\phi < \phi_c(\omega)$. For fixed ω, $\phi_c(\omega)$ separates volume fraction into 2 regimes: the "walking" regime ($\phi \geq \phi_c$, $\bar{v}_x \gg 0$) and the "swimming" regime ($\phi < \phi_c(\omega)$, $\bar{v}_x \approx 2$ cm/s). See Movie S4 and Movie S5 for examples of rotary walking and swimming modes.

The rotary walking mode is dominant at low ω and high ϕ. In this mode, a tripod of limbs penetrates down and backward into the ground until the granular yield stress exceeds the limb transmitted inertial, gravitational, and frictional stresses at a depth $d(\omega, \phi)$. At this point, rather than rolling forward like a wheel, the c-leg abruptly stops translating relative to the grains and begins slipping tangentially in the circular depression surrounding it; at the same time, the center of rotation moves from the axle to the now stationary center of curvature (see Fig. 3*A*). The simultaneous halt in both vertical and horizontal leg motion is apparently due to the large reduction in belly friction forces that occurs when the weight of the robot is supported by the limbs rather than the underside of the body or the other tripod. The ensuing rotary motion propels the axle and consequently the rest of the robot body along a circular trajectory in the x–z plane with speed $R\omega$, where $R = 3.55$ cm is the c-leg radius. The forward body motion ends when, depending on ϕ and ω, either
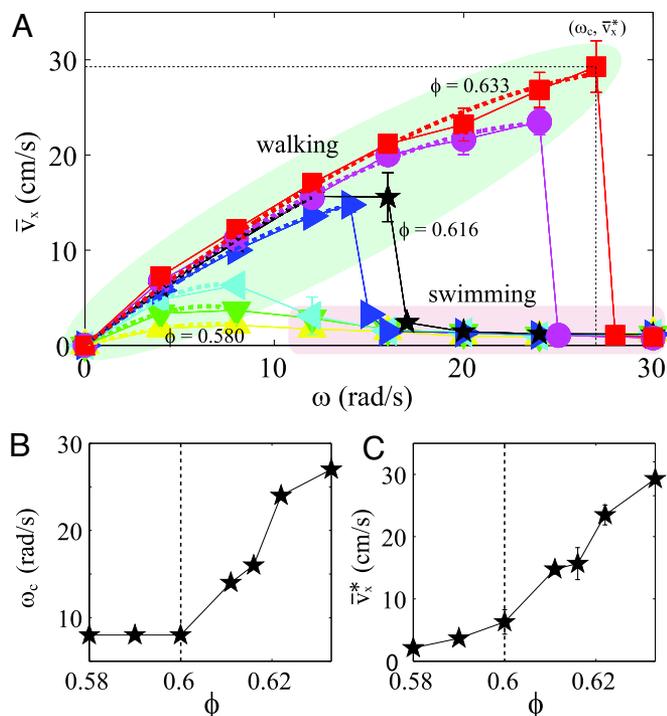
Fig. 2. Average robot speed vs. limb frequency. (*A*) For a given volume fraction ϕ, $\bar{v}_x$ increases sublinearly with ω to a maximal average speed $\bar{v}_x^*$ at a critical limb frequency ω_c above which the robot swims ($\bar{v}_x \approx 2$ cm/s). The solid lines and symbols are for $\phi = 0.580, 0.590, 0.600, 0.611, 0.616, 0.622,$ and 0.633. The dashed lines are fits from a simplified model discussed in the text. (*B* and *C*) The dependence of ω_c and $\bar{v}_x^*$ on ϕ shows transitions at $\phi \approx 0.6$ (dashed lines).

the second tripod begins to lift the robot or the underside of the robot contacts the ground.

With increased ω, limbs penetrate further as the requisite force to rapidly accelerate the robot body to the finite limb speed ($R\omega$) increases. As the penetration depth approaches its maximum $2R - h$, where $h = 2.5$ cm is the height of the axle above the flat underside of the robot, the walking step size goes to zero because there is no longer a point in the cycle where the limb ceases its motion relative to the grain bed. Any subsequent forward motion is due solely to thrust forces generated by the swimming-like relative translational motion of the limb through the grains. Note that $\phi_c(\omega)$ increases with ω, and that the transition from rotary walking to swimming is sharper in $\bar{v}_x$ for higher ω and smoother for lower ω. The much slower swimming mode occurs for all volume fractions for $\omega \gtrsim 28$ rad/s.

Plotting the average robot speed as a function of limb frequency (Fig. 2*A*) shows that the robot speed increases sublinearly as its legs rotate more rapidly. For fixed ϕ, $\bar{v}_x$ increases sublinearly with ω to a maximal speed $\bar{v}_x^*$ at a critical limb frequency ω_c, above which $\bar{v}_x$ quickly decreases to ≈ 2 cm/s (swimming). Performance loss for $\phi \gtrsim 0.6$ is sudden ($\Delta\omega \approx 1$ rad/s) compared with performance loss for $\phi \lesssim 0.6$. Both ω_c and $\bar{v}_x^*$ display transitions at $\phi \approx 0.6$ (Fig. 2 *B* and *C*). The transition at $\phi \approx 0.6$ for the rapidly running robot is noteworthy because it has been observed that granular media undergo a transition in quasistatic penetration properties at $\phi \approx 0.6$ (29).

Starting with the observed kinematics of rotary walking with circular slipping, we constructed a straightforward 2-parameter model that captures the essential elements determining granular locomotion for our legged device and agrees well with the data (dashed lines in Fig. 2*A*). The model, which incorporates simplified kinematics and granular penetration forces while still agreeing well with a more realistic treatment (for a more detailed

discussion of the model, see *Materials and Methods*), indicates that reduction of step length through increased penetration depth is the cause of the sublinear increase in $\bar{v}_x$ with ω and the rapid loss of performance above ω_c. The model assumes that the 2 tripods act independently, that the motion of each tripod can be understood by examining the motion of a single c-leg supporting a mass m equal to one-third of SandBot's total mass and that the underside of the robot rests on the surface at the beginning of limb-ground contact.

Using the geometry of rotary walking (see Fig. 3*A*), the walking step length per c-leg rotation is $s = 2\sqrt{R^2 - (d + h - R)^2}$, where d is the maximum depth of the lowest point on the leg. After the robot has advanced a distance s, the body again contacts the ground and the c-leg moves upward. Because during each clock signal period there are two leg rotations (1 for each tripod), the average horizontal velocity is $2s \times$ limb frequency or $\bar{v}_x = \frac{\omega s}{\pi}$. The maximum limb penetration depth d is thus the key model component because it controls the step length (see Fig. 3*B*) and consequently the speed. Maximum limb penetration depth is determined by balancing the vertical acceleration of the robot center of mass ma with the difference of the gravitational force mg and the vertical granular penetration force kz (30), where g is the acceleration due to gravity, and $k(\phi)$ is a constant characterizing the penetration resistance of the granular material of volume fraction ϕ.

At small ω, $-ma \approx 0 = \Sigma F_i = mg - kd$, so $d = mg/k$, which is the minimum penetration depth. For finite ω, the penetration depth is greater because an additional force must be supplied by the ground to accelerate the robot body to the leg speed $R\omega$ when the c-leg stops translating in the material. Taking $a = \Delta v/\Delta t$, with $\Delta v = R\omega - 0$ and Δt the characteristic elastic response time of the limb and grain bed, gives the acceleration magnitude $a = R\omega/\Delta t$. The direction of the acceleration depends on the position of the c-leg. To keep the model simple, we approximate the vertical component of the acceleration with its magnitude. Equating the vertical forces with mass $\times$ acceleration (see Fig. 3*C*), $-m\frac{R\omega}{\Delta t} = mg - kd$, gives c-leg penetration $d = \frac{m}{k}(\frac{R\omega}{\Delta t} + g)$ with average horizontal velocity

$$\bar{v}_x = \frac{2R\omega}{\pi}\sqrt{1 - \left[\frac{m}{k(\phi)}\left(\frac{\omega}{\Delta t} + \frac{g}{R}\right) + \frac{h}{R} - 1\right]^2}.$$

Fits of the experimental data to this model are indicated by dashed lines in Fig. 2*B*. The expression captures the sublinear increase in $\bar{v}_x$ with ω at fixed $k(\phi)$, the increase in speed at fixed ω as the material strengthens (increasing k with increasing ϕ), and the limit of zero rotary walking speed when ω is sufficiently large.

The expression for $\bar{v}_x$ is determined by the fit parameters k and Δt. The parameter k characterizing the penetration resistance increases monotonically with ϕ from 170 to 220 N/m and varies rapidly below $\phi \approx 0.6$ and less rapidly above. Its average value of ≈ 200 N/m corresponds to a shear stress per unit depth of $\alpha \approx 470$ kN/m³ (using leg area $= wR$, where w is the leg width) which is in good agreement with penetration experiments we performed on poppy seeds that yield $\alpha = 300$ and 480 kN/m³ for $\phi = 0.580$ and 0.622, respectively, and is comparable with previous measurements of slow penetration into glass beads (31), where $\alpha \approx 250$ kN/m³. In contrast, Δt varies little with ϕ and has an average value of 0.4 s compared with the robot's measured hard ground oscillation period of 0.2 s when supported on a single tripod. The differences in Δt can be understood as follows. In our model we assume the 2 tripods do not simultaneously contact the ground; however, in soft ground this is not the case, which consequently reduces the effective step length per period from $2s$ to a lesser value. The fit value of Δt is sensitive to this variation;
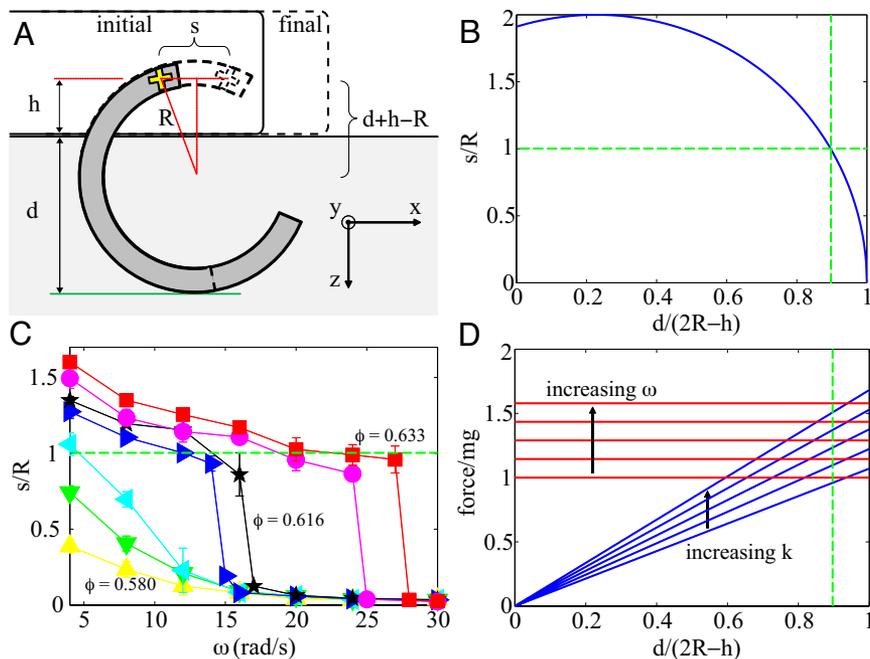
Fig. 3. Robot speed is determined by step size which depends sensitively on c-leg penetration depth. (*A*) Schematic of a single robot leg during a step in granular media. After reaching penetration depth *d*, the leg rotates about its center and propels the robot forward a step length *s*. The solid shape denotes the initial stage of the rotational motion and the dashed shape indicates when the limb begins to withdraw from the material (end of forward body motion). (*B*) Step length vs. penetration depth (blue) with critical step length (green dashed horizontal) and critical penetration depth (green dashed vertical) indicating where the robot begins to encounter ground disturbed by the previous step. (*C*) Granular penetration force for $k = 1.75, 2.00, 2.25, 2.50, 2.75 \times 10^5$ N/m (blue) and force required to initiate rotary walking for $\omega = 0, 8, 16, 24, 32$ rad/s (red) vs. penetration depth using simplified walking model with $\Delta t = 0.2$ s. The penetration depth at constant ϕ is determined by the intersections of the corresponding blue line with the red lines. Beyond the critical depth (green dashed line) limbs encounter disturbed material and move to lower blue lines. (*D*) Step length as a function of ω derived from $2s = 2\pi\bar{v}/\omega$ reveals the condition for the onset of swimming for $\phi \gtrsim 0.6$ as $s/R \approx 1$. The solid lines and symbols are for ϕ values of 0.580, 0.590, 0.600, 0.611, 0.616, 0.622, and 0.633.

reducing the step size (and thus the speed) in the experimental data by just 13% decreases Δt to 0.2 s, whereas k is increased by <10%.

Our model indicates that for deep penetration, the walking step length is sensitive to penetration depth (e.g., Fig. 3*B*). As the walking step length goes to zero with increasing ω or decreasing ϕ, the fraction of the ground contact time that the leg slips through the grains (swimming) goes to 1. Swimming in granular media differs from swimming in simple fluids because the friction dominated thrust and drag forces are largely rate independent at slower speeds (30, 32). When thrust exceeds drag and using constant acceleration kinematics, the robot advances a distance proportional to the net force divided by ω^2 per leg rotation, and, consequently, speed is proportional to ω^{-1}. This explains the weak dependence of $\bar{v}_x$ on ω in the swimming mode. The increase in robot speed with decreasing ω is bounded by the condition that the robot speed in a reference frame at rest with respect to the ground cannot exceed the horizontal leg speed in a reference frame at rest with respect to the robot's center of mass. This condition ensures the existence of and eventual transition to a walking mode as ω is decreased.

The transition from walking to swimming appears gradual for $\phi \lesssim 0.6$ because the penetration depth increases slowly with ω at small ω ($R\omega/\Delta t \ll g$) and the ω^{-2} contribution to the per-cycle displacement from swimming is relatively large (see, e.g., the data at $\omega = 12$ rad/s in Fig. 3*B*). However, for $\phi \gtrsim 0.6$, the transition is abrupt. This sharp transition occurs because the step size is reduced sufficiently that the legs encounter material disturbed by the previous step; we hypothesize that the disturbed material has lower ϕ and k. At higher ϕ, the volume fraction of the disturbed ground is significantly less than the bulk, which increases penetration and consequently greatly reduces s. This is not the case for the transition from walking to swimming at lower ϕ (and low ω) where the volume fraction of the disturbed material is largely unchanged relative to its initial value. For the robot to avoid disturbed ground, it must advance a distance R on each step, i.e., $s \geq R$, or in terms of the penetration depth, $d \leq (\sqrt{3}/2 + 1)R - h = 5.0$ cm (green dashed lines in Fig. 3 *B* and *C*). The disturbed ground hypothesis is supported by calculations of the step length derived from the average velocity $2s = 2\pi\bar{v}_x/\omega$, which show a critical step length near $s/R = 1$ at the walking/swimming transition (Fig. 3*D*) for $\phi \gtrsim 0.6$. The somewhat smaller value of $s/R \approx 0.9$ evident in the figure can be understood by recognizing that for s slightly smaller than R the majority of the c-leg still encounters undisturbed material. Signatures of the walking/swimming transition are also evident in lateral views of the robot kinematics (see Movie S3, Movie S4, and Movie S5).

At higher ω in the swimming mode, limbs move with sufficient speed to fling material out of their path and form a depression that reduces thrust because the limbs are not as deeply immersed on subsequent passes through the material. However, as limb speed increases further, thrust forces become rate dependent and increase because the inertia imparted to the displaced grains is proportional to ω^2. Between strokes, the excavated depression refills at a rate that depends on the difference between the local surface angle and the angle of repose (33), and the depression size. Investigating the competition between these different processes at high ω, and their consequences for locomotion could be relevant to understanding how to avoid becoming stranded or to free a stranded device.

Conclusions

Our study systematically investigates the performance of a legged robot on granular media, varying both properties of the

medium (volume fraction) and properties of the robot (limb frequency and gait). Our experiments reveal how precarious it can be to move on granular media: changes in ϕ of $<1\%$ result in either rapid motion or failure to move, and slight kinematic changes have a similar effect. A kinematic model captures the speed dependence of SandBot on granular material as a function of ϕ and ω. The model reveals that the sublinear dependence of speed on ω and the rapid failure for sufficiently small ϕ and/or large ω are consequences of increasing limb penetration with decreasing ϕ and/or increasing ω, and changes to local ϕ due to penetration and removal of limbs. Although detailed studies of impact and penetration of simple rigid objects exist (30, 34), further advances in performance (including increases in efficiency) and design of limb morphology will require a more detailed understanding of the physics associated with penetration, drag, and crater formation and collapse, especially their dependence on ϕ. Better understanding of this physics can guide development of theory of interaction with complex media advanced enough to predict limb design (35) and control (36) strategies, similar to the well-developed models of aerial and aquatic craft. Analysis of physical models such as SandBot can also inform locomotion biology in understanding how animals appear to move effortlessly across a diversity of complex substrates (25, 37). Such devices will begin to have capabilities comparable with organisms; these capabilities could be used for more efficient and capable exploration of challenging terrestrial (e.g., rubble and disasters sites) and extraterrestrial (e.g., the Moon and Mars) environments.

Materials and Methods

Limb Kinematics. SandBot's 6 motors are controlled by a clock signal to follow the same prescribed kinematic path during each rotation and, as shown in previous work on RHex, changes in these kinematics have substantial effects on robot locomotor performance (38). The controlling clock signal consists of a fast phase and a slow phase with respective angular frequencies. The fast phase corresponds to the swing phase, and the slow phase corresponds to the stance phase. A set of 3 gait parameters uniquely determines the clock signal configuration: θ_s, the angular span of the slow phase; θ_0, the leg-shaft angle of the center of the slow phase; and d_c, the duty cycle of the slow phase. Specifying the cycle average limb angular frequency ω fully determines the limb motion.

In pilot experiments, we tested 2 sets of clock signals: a hard ground clock signal (HGCS) with ($\theta_s = 0.85$ rad, $\theta_0 = 0.13$ rad, $d_c = 0.56$) which generates a fast bouncing gait (60 cm/s) on hard ground (17) but very slow (≈ 2 cm/s) motion on granular media, and a soft ground clock signal (SGCS) with ($\theta_s = 1.1$ rad, $\theta_0 = -0.5$ rad, $d_c = 0.45$) which produces unstable motion on hard ground but regular motion on granular media. These experiments showed that the locomotor capacity of SandBot is sensitive to the clock signal. Careful observation of limb kinematics revealed that the HGCS fails on granular media because of the simultaneous stance phase of 2 tripods. In this study, we use SGCS and explore robot performance as a function of limb frequency and substrate volume fraction.

Integrated motor encoders record the position and current (and thus torque) of SandBot's motors vs. time. Comparison of the measured and prescribed angular trajectories for both sets of gait parameters show a high degree of fidelity with an error of a few percent. Therefore, SandBot's change in performance between HGCS and SGCS timing comes from the physics of the substrate interaction.

Trackway Volume Fraction Control. To systematically test SandBot's performance vs. substrate volume fraction, we employ a 2.5-m-long, 0.5-m-wide fluidized bed trackway with a porous plastic (Porex) flow distributor (thickness 0.64 cm, average pore size 90 μm). Four 300-L/min leaf blowers (Toro) provide the requisite air flow. Poppy seeds are chosen as the granular media because they are similar in size to natural sand (39) and are of low enough density to be fluidized. The air flow across the fluidized bed is measured with an anemometer (FMA-900-V; Omega Engineering) and is uniform to within 10%.

A computer controlled fluidization protocol sets the volume fraction and thus the mechanical properties of the granular media. A continuous air flow initially fluidizes the granular media in the bubbling regime. The flow is slowly turned off, leaving the granular media in a loosely packed state ($\phi = 0.580$). Short air pulses (ON/OFF time = 0.1/1 s) pack the material (28). Increasing the number of pulses increases ϕ up to a maximum of $\phi = 0.633$. Volume fraction is calculated by dividing the total grain mass by the bed volume and the
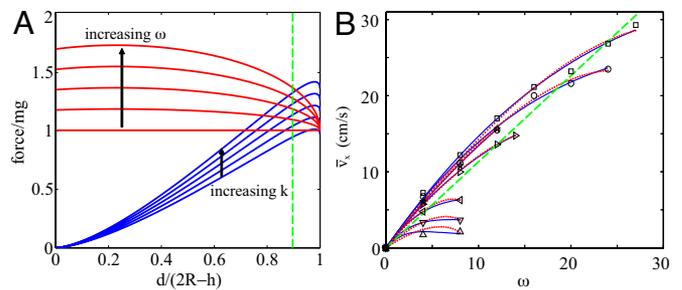
Fig. 4. Comparison of detailed model dynamics with simple model and experiment. (*A*) Nondimensionalized granular force (blue curves) for $\alpha = 250$, 275, 300, 325, and 350 kN/m^3 and the required force to initiate rotary walking, $a_z/g + 1$ (red curves) for $\omega = 0$, 7.5, 15, 22.5, 30 rad/s for the full model as a function of limb penetration depth with a 225° c-leg arc angle and $\Delta t = 0.15$ s. The intersection of the red and blue curves determines the penetration depth of the limb and consequently the step length. At constant material strength (blue) d increases with increasing ω, whereas at constant ω, increasing material strength reduces d. The vertical green dashed line indicates the critical penetration depth beyond which the leg encounters material disturbed by the previous step. (*B*) Comparison of $\bar{v}_x$ vs. ω for simple (red dotted curve) and full (blue solid curve) models. Models are fit to the measured robot speed (symbols) for $\bar{v}_x \leq \bar{v}_x^*$. The green dashed line indicates $\bar{v}_x^* = R\omega/\pi$ or equivalently $s = R$. In *A* and *B*, $h = 2.5$ cm, $R = 3.55$ cm, $w = 1.2$ cm, and $m = 767$ g.

intrinsic poppy seed density. The mass is measured with a precision scale (Setra). The density of the granular media is measured by means of displacement in water. In experiment, because the horizontal area of the fluidized bed trackway is fixed, volume fraction is set by controlling the height of the granular media (e.g., volume = area × height).

Kinematics Measurements. To characterize SandBot's motion, we record simultaneous dorsal and lateral views with synchronized high speed video cameras (AOS) at 100 frames per second. The center of mass (dorsal landmark) and the axles of the right-side front and rear motors (lateral landmarks) are marked with reflective material (Wite-Out). A rail-pulley system allows the robot's power and communication cables to follow the robot as it moves to minimize the drag from the cables. For each trial, we prepare the trackway with the desired volume fraction and place the robot on the prepared granular media at the far end of the trackway with both tripods in the same standing position. An LED on the robot synchronizes the video and robot motor encoder data. After each trial, MATLAB (MathWorks) is used to obtain landmark coordinates from the video frames and calculate $v_x(t)$. Three trials were run for each combination of (ϕ,ω) that was tested.

Detailed Discussion of Rotary Walking Locomotion Model. The model presented in the main body of the manuscript simplifies the underlying physics while capturing the essential features determining robot speed. Here, we describe a more complete model (which lacks a simple expression for $\bar{v}_x$) and compare its predictions to those of the simple model. The exact expression for the vertical acceleration component of the body when the limbs gain purchase is $ma_z = ma \sin\theta = ma \sqrt{2(h + z)/R - (h + z/R)^2}$ instead of the approximation $ma_z = ma$ used in the simple model. Using the exact expression, the vertical granular force necessary for walking still has the same peak value of $m(a + g)$ but decreases to mg when the limb is at its lowest point.

The second approximation we used in the simple model is that the grain force on the leg is kz. This expression is only strictly valid for a flat-bottomed vertically penetrating intruder (30). Because the leg is a circular arc, the leg-grain contact area and the vertical component of the grain force are functions of limb depth and leg-shaft angle. Generalizing kz to a local isotropic yield stress given by αz (12), the vertical force on a small segment of the limb $Rd\psi$ in length at depth z is $dF_z = w\alpha z Rd\psi\cos\psi$, where w is the limb width and ψ the angular position of the segment with respect to a vertical line passing through the axle. The total vertical component of the force acting on the leg is then $Rw\alpha\int_{-\psi_{min}}^{\psi_{max}} z\cos\psi d\psi$. Substituting $z(\psi) = R(\cos\psi - 1) + d$ and integrating gives $F_z = Rw\alpha \left[\frac{R}{2}(\psi + \cos\psi\sin\psi) + (d - R)\sin\psi\right]_{-\psi_{min}}^{\psi_{max}}$, where $\psi_{max} = \cos^{-1}(1 - d/R)$ and $\psi_{min} = \psi_{max}$ when the leg tip is above the center of the c-leg and $\psi_{min} = \cos^{-1}(\frac{d + h}{R} - 1) + \Delta\xi$ when it is below the center of the c-leg. $\Delta\xi$ is the angular extent of the limb beyond π (e.g., $\Delta\xi = 0$ for a semicircular limb).

Fig. 4*A* shows that the full model using realistic parameters shares the same essential physics as the simple model. For a given material strength (blue

PHYSICS

curves), the penetration depth increases with increasing ω (intersection of blue and red curves) until the step length is reduced below the critical value (vertical green dashed line). Fig. 4B presents fits to the experimental data of the average speed $\bar{v}_x$ vs. ω for the full and simple models for $v_x \le \bar{v}_x^*$ at each ϕ. The fits and fit parameters for the simple ($\bar{\Delta}t = 0.4$ s, $\bar{\alpha} = 470$ kN/m^3) and full ($\bar{\Delta}t = 0.2$ s, $\bar{\alpha} = 330$ kN/m^3) models are in good agreement when the step length is less than the critical value s = R.

1. Kumagai J (2004) Sand trip—DARPA's 320-kilometer robotic race across the Mojave Desert yields no winner, but plenty of new ideas. *IEEE Spectrum* 41:44–50.
2. Raibert MH (1986) Legged robots. *Commun ACM* 29:499–514.
3. Bekker M (1956) *Theory of Land Locomotion* (Univ of Michigan Press, Ann Arbor, MI), p 520.
4. Kadanoff LP (1999) Built upon sand: Theoretical ideas inspired by granular flows. *Rev Mod Phys* 71:435–444.
5. Altendorfer R, Koditschek DE, Holmes P (2004) Stability analysis of legged locomotion models by symmetry-factored return maps. *Int J Robotics Res* 23:979–999.
6. Westervelt ER, Buche G, Grizzle JW (2004) Experimental validation of a framework for the design of controllers that induce stable walking in planar bipeds. *Int J Robotics Res* 23:559–582.
7. Cavagna GA, Heglund NC, Taylor CR (1977) Mechanical work in terrestrial locomotion—2 basic mechanisms for minimizing energy-expenditure. *American Journal of Physiology* 233:R243–R261.
8. Berkemeier MD, Fearing RS (1998) Sliding and hopping gaits for the underactuated acrobot. *IEEE Transact Robotics Automation* 14:629–634.
9. Schmitt J, Holmes P (2000) Mechanical models for insect locomotion: dynamics and stability in the horizontal plane I. Theory. *Biological Cybernetics* 83:501–515.
10. Ezcurra E (2006) *Global Deserts Outlook* (United Nations, New York), p 168.
11. Terzaghi K (1943) *Theoretical Soil Mechanics* (Wiley, New York), p 510.
12. Nedderman R (1992) *Statics and Kinematics of Granular Materials* (Cambridge Univ Press, Cambridge, UK), p 352.
13. Heil P, Rericha EC, Goldman DI, Swinney HL (2004) Mach cone in a shallow granular fluid. *Phys Rev E* 70:060301–060304.
14. van Zon JS, et al. (2004) Crucial role of sidewalls in velocity distributions in quasi-two-dimensional granular gases. *Phys Rev E* 70:040301–040304.
15. Goldman DI, Swinney HL (2006) Signatures of glass formation in a fluidized bed of hard spheres. *Phys Rev Lett* 96:174302–174305.
16. Goldman DI, Korff WL, Wehner M, Berns MS, Full RJ (2006) The mechanism of rapid running in weak sand. *Integr Comp Biol* 46:E50.
17. Saranli U, Buehler M, Koditschek DE (2001) Rhex: A simple and highly mobile hexapod robot. *Int J Robotics Res* 20:616–631.
18. Koditschek DE, Full RJ, Buehler M (2004) Mechanical aspects of legged locomotion control. *Arthropod Struct Dev* 33:251–272.
19. Blickhan R, Full RJ (1993) Similarity in multilegged locomotion: Bouncing like a monopode. *J Comp Physiol A* 173:509–517.
20. Holmes P, Full RJ, Koditschek DE, Guckenheimer J (2006) The dynamics of legged locomotion: Models, analyses, and challenges. *Soc Industr Appl Math Rev* 48:207–304.
21. Ritzmann RE, Quinn RD, Fischer MS (2004) Convergent evolution and locomotion through complex terrain by insects, vertebrates and robots. *Arthropod Struct Dev* 33:361–379.
22. Kim S, Clark JE, Cutkosky MR (2006) iSprawl: Design and tuning for high-speed autonomous open-loop running. *Int J Robotics Res* 25.
23. Playter R, Buehler M, Raibert M (2006) BigDog, *Proceedings of SPIE*, ed Gerhart GR, Shoemaker CM, Gage DW (SPIE, San Diego), Vol 6230, pp 62302O1–62302O6.
24. McBride B, Longoria R, Krotkov E (2003) in *Measuring the Performance and Intelligence of Systems: Proceedings of the 2003 PerMIS Workshop*, eds Messina E, Meystel A, (National Institute of Standards and Technology, Gaithersburg, MD), pp 405–412.
25. Spagna JC, Goldman DI, Lin PC, Koditschek DE, Full RJ (2007) Distributed mechanical feedback in arthropods and robots simplifies control of rapid running on challenging terrain. *Bioinspir Biomimetics* 2:9–18.
26. Altendorfer R, et al. (2001) Rhex: A biologically inspired hexapod runner. *Auton Robots* 11:207–213.
27. Jackson R (2000) *The Dynamics of Fluidized Particles* (Cambridge Univ Press, Cambridge, UK), p 339.
28. Schroter M, Goldman DI, Swinney HL (2005) Stationary state volume fluctuations in a granular medium. *Phys Rev E* 71:030301–030304.
29. Schroter M, Nagle S, Radin C, Swinney HL (2007) Phase transition in a static granular system. *Europhys Lett* 78:44004–44007.
30. Albert R, Pfeifer MA, Barabasi AL, Schiffer P (1999) Slow drag in a granular medium. *Phys Rev Lett* 82:205–208.
31. Stone MB, et al. (2004) Local jamming via penetration of a granular medium. *Phys Rev E* 70:041301–041310.
32. Wieghardt K (1975) Experiments in granular flow. *Annu Rev Fluid Mech* 7:89–114.
33. de Vet S, de Bruyn J (2007) Shape of impact craters in granular media. *Phys Rev E* 76:041306–041311.
34. Goldman DI, Umbanhowar P (2008) Scaling and dynamics of sphere and disk impact into granular media. *Phys Rev E* 77:021308–021321.
35. Santos D, Spenko M, Parness A, Kim S, Cutkosky M (2007) Directional adhesion for climbing: theoretical and practical considerations. *J Adhes Sci Technol* 21:1317–1341.
36. Hodgins JK, Raibert MH (1991) Adjusting step length for rough terrain locomotion. *IEEE Transact Robotics Automat* 7:289–298.
37. Goldman DI, Chen TS, Dudek DM, Full RJ (2006) Dynamics of rapid vertical climbing in cockroaches reveals a template. *J Exp Biol* 209:2990–3000.
38. Weingarten J, Lopes GAD, Buehler M, Groff RE, Koditschek DE (2004) Automated Gait Adaptation for Legged Robots. *Robotics and Automation 2004*, (Institute of Electrical and Electronics Engineers, Piscataway, NJ), pp 2153–2158.
39. Bagnold RA (1954) *The Physics of Blown Sand and Desert Dunes* (Methuen, London), p 265.
40. Dickinson WW, Ward JD (1994) Low depositional porosity in Eolian sands and sandstones, Namib desert. *J Sediment Res A Sediment Petrol Process* 64:226–232.
41. Full RJ, Koditschek DE (1999) Templates and anchors: Neuromechanical hypotheses of legged locomotion on land. *J Exp Biol* 202:3325–3332.

Li *et al.*

Movies

1. Control of Granular Media Compaction by Air Fluidized Bed

2. SandBot Gaits

3. SandBot Stuck with Gait Tuned for Solid Ground

4. SandBot Moving with Gait Tuned for Granular Media

5. SandBot on Granular Media of Different Compactions

6. SandBot Walking Mode

7. SandBot Swimming Mode